International Journal of Earth Sciences Knowledge and Applications
journal homepage: http://www.ijeska.com/index.php/ijeska
e-ISSN: 2687-5993

Research Article https://doi.org/10.5281/zenodo.17020942

Granulometric and Geochemical Analyses of Stream Sediments from Part of Southwestern Nigeria: Implication for Mineralization Potential

O.S. Bamigboye[1,2]*, O.A. Omorinoye[2], T.E. Bamidele[1], H.A. Umar[1]
[1]Department of Geology and Mineral Sciences, Kwara State University, Malete, Nigeria
[2]Department of Geology and Mineral Sciences, University of Ilorin, Ilorin, Nigeria

Article history
Received 06 March 2025
Accepted 25 April 2025
Published 30 April 2025

Contact
*O.S. Bamigboye
olufemi.bamigboye@kwasu.edu.ng (OSB)

How cite
Bamigboye, O.S., Omorinoye, O.A., Bamidele, T.E., Umar, H.A., 2025. Granulometric and Geochemical Analyses of Stream Sediments from Part of Southwestern Nigeria: Implication for Mineralization Potential. International Journal of Earth Sciences Knowledge and Applications 7 (1), 208-222. https://doi.org/10.5281/zenodo.17020942.

Abstract
This work investigates the mineralization potential of an area bounded by longitude 4° 52′ to 5° 00′ E and latitude 8° 22′ to 8° 28′N represented on Ilorin Sheet 223. The methods adopted in this work include field mapping, granulometric, heavy mineral, stream sediment and statistical analyses. The result of the granulometric analysis reveals that the sediments range from very coarse sand to coarse sand, are poorly sorted and exhibit very platykurtic distribution. The result of Factor Analysis identified eight distinct Factor groups. Factor 1 of the group was interpreted to be related to hydrothermal sulphide ore mineralization that is complex and formed at low temperature, while Factor 2 is interpreted to imply gold-associated gangue minerals. Factor 3 was interpreted to indicate the presence of a vein deposit that is mafic in composition, while Factors 7 and 8 were interpreted to indicate the presence of low temperature hydrothermal sulphide mineralization. Heavy minerals identified in the samples include zircon, sillimanite, goethite, hematite and olivine among others. The conclusion drawn from this work is that the southeastern and northwestern parts of the study area have enhanced ore-forming elements; hence, the area is mineralized with pockets of such sulphide. The northeastern part is barren. It was also concluded that exploratory work should focus on the southeastern and northwestern parts of the area. In addition, mineralization in the area consists mainly of low-temperature hydrothermal sulphide ore deposits, including gold.

Keywords
Granulometric analysis, mineralization, heavy mineral, geochemistry, geology

1. Introduction

Stream sediment geochemistry gained wide acceptability in mineral exploration in the period between 1930 and 1960 because of the invention of rapid and sensitive methods of determining a wide variety of trace elements in earth materials. These sediments also provide easily detectable alluvial dispersion trains of valuable minerals and metals along the stream channel that provides effective exploration guides (Jun et al., 2024; Zhihua et al., 2024; Adam et al., 2023; Bamigboye and Adekeye 2011; Adekeye, 1999).

Analysis of these sediments and careful study of the resistance minerals can help in tracing the source(s) of the minerals and or heavy minerals in the stream sediments up-stream. Olayinka and its environs bordered by longitude 4° 52′ to 5° 00′ E and latitude 8° 22′ to 8° 28′N is part of the Basement Complex of southwestern Nigeria represented on Ilorin Sheet 223. The surrounding settlements include but are not limited to Agunjin, Igbaja, Alla, Obi-Igbaja among others. Bamigboye et al. (2023) probed the mineralization potential of Ilorin Sheet 223 using aeromagnetic and aero-radiometric techniques. From their work, the geology of the areas represented on this sheet is made-up of migmatite, geniuses, quartzites, schist and granites while the rocks that dominate the northwestern part of the area have relatively higher hydrothermal alterations. Their study revealed a consistent NE-SW lineament orientation across the area. While the presence of artisanal miners has been reported in

Agunjin and Alla, none is heard of in Olayinka and its environs that are within the same area. Furthermore, this area has remained uninvestigated and there is no available formal documentation on the potential of mineralization in the area. This work is therefore aimed at investigating the mineralization potential of Olayinka and its environs using stream sediment geochemistry. The objective of this work is firstly to delineate the mineralized zone from the barren zone. Secondly, to characterize the sediments and their depositional characteristics. Lastly, to affirm the type of mineralization that is present in the area.

The Basement Complex of Nigeria covers about half of the total surface area of Nigeria while the sedimentary rocks cover the remaining half. Lithologically, the Basement Complex of Nigeria has been described to consist of the Migmatite-Gneiss-Quartzite Complex, the Older Granite, and the Younger Granite (Russ, 1957; Truswell and Cope, 1963; Oyawoye, 1972; Jones and Hockey, 1964; Rahaman, 1988; McCurry and Wright, 1977; Rahaman and Ocan, 1978; Ekwueme and Shing, 1987).

The Migmatite-Gneiss-Quartzite Complex has lithologies that include the migmatite-gneiss that is further subdivided into biotite gneiss and the banded gneiss; quartzite, marble and other calcareous rocks including relics of metamorphosed clayey sediments but lithologies of the Older Granite include migmatitic gneiss, granite gneiss, early pegmatite, fine grained granite, homogeneous to coarse grained granite, slightly deformed pegmatite, aplites and vein quartz and undeformed pegmatite. Younger Granite is distinguished from the Older Granite based on the age of emplacement and its tin mineralization. Its occurrence is in the Jos area of Nigeria.

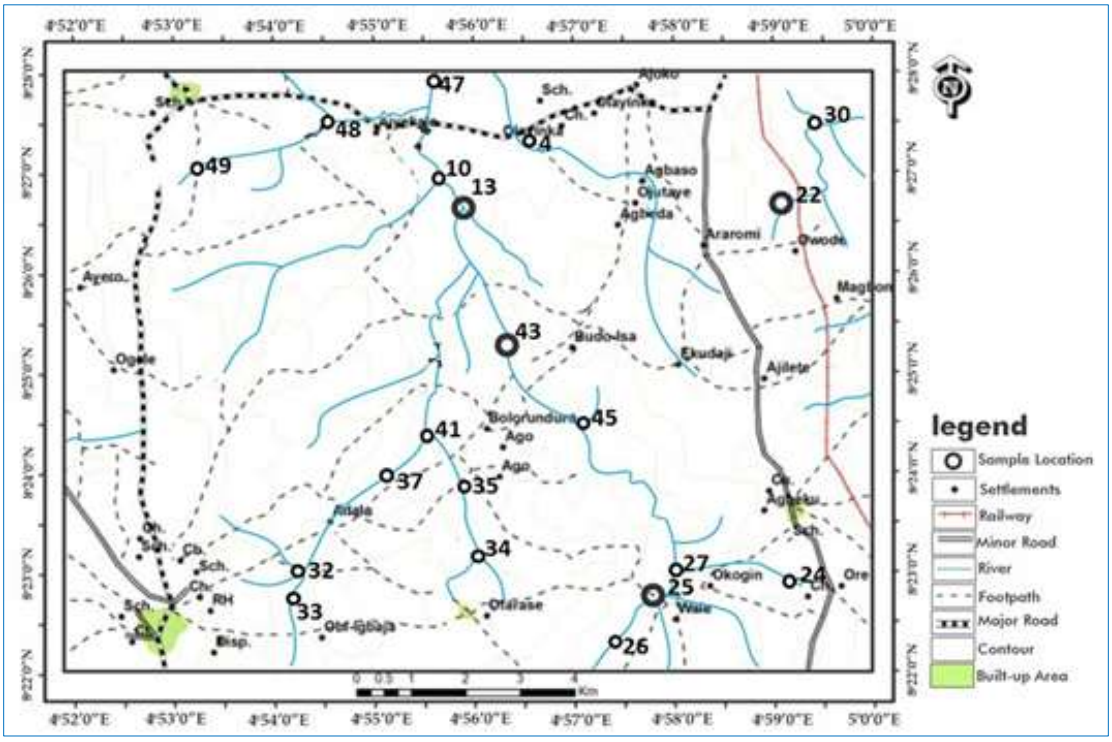

Fig. 1. Topographical map of the area showing sample locations

The Basement Complex is divided into three blocks; these are in the north-central where it is circular in outline, in the southeast and in the southwestern part where it is triangular. The mineralization potential of these blocks has been assessed by different authors using different techniques. Some of these include but are not limited to remote sensing, integrated geophysical methods, petrology, and geochemistry. Stream sediment geochemical survey is one of the methods that have been extensively used in probing the Basement Complex of Nigeria for her mineralization.

Awosusi et al. (2019) assessed the mineralization potential of area drained by Rivers Iyinsi and Ofosu from the geochemical data of the stream sediment using R-Mode Factor Analysis. The result of their statistical analysis of the geochemical data cumulated into six-factor models. Their Factors 3, 5 and 6 were interpreted to be related to gold and associated sulphide minerals, and Fe and Mn-oxides mineralization.

Adekoya et al. (2021) did a reconnaissance stream sediment geochemical survey of Uokha Area, southwestern, Nigeria with the aim of isolating potentially mineralized area from the barren one. A total of sixty stream sediment samples were analyzed for thirteen elements. The result of their geochemical analysis was subjected to statistical analyses. From the results, Factors 2 and 3 were interpreted to be related to gold and tin mineralization even though the elements are long-distributed and the cumulative probability plots of their elements, except Cd and Zn, exhibited multiple populations. This implied the occurrence of both background and anomalous values.

Obaje and Pirisola (2023) conducted geochemical characterization of Egbetua stream sediments, southwestern Nigeria to determine the provenance and depositional conditions of the sediments.

Key parameters analyzed included the Chemical Index of Alteration (CIA), element distribution, stream flow energy, and depositional condition. It was concluded by the CIA that the sediments are of felsic source while the prevailing condition of deposition is reducing oxidizing even though, their calculated Ce/Ce confirmed and an oxidizing environment of deposition with low stream flow energy. This is supported by their Eu/Eu that attested to oxidizing environment with felsic source.

2. Methodology

The field mapping exercise was carried out in December 2019. It entails traversing the study area with the aid of Silva compass clinometers and eTrex GPS. To effectively cover the area, the topographical map was gridded. At each location, the outcrops were carefully examined and properly located on the base map for digitization using Global Positioning System (GPS). Structural features such as foliations, joints, mineral lineation, intrusions, faults, and folds (rarely encountered on the outcrops) were recorded in the field note. Based on in-situ observations of textural and compositional characteristics of the outcrop, tentative names were given to rock samples collected. A total of twenty-five stream sediment samples were collected at the confluence of two or more first order streams and or on rare occasions, first and second order streams. For a long stream channel, sample was taken at the meandering point. Geologically, these sediments are Recent in age because they were deposited within a year prior to the sampling date.

The stream sediments were sundried and disaggregated. For granulometric analysis, 100 g of the sediments were weighed and subjected to dry-sieved (See Table 1a for details of the mesh sizes); 20 samples that were representative and evenly spread over the area were pulverized for elemental analysis using an agate mortar and pestle while 25 samples were subjected to heavy mineral analysis. The geochemical analysis was done at MS Analytical laboratory, Canada. In the laboratory, samples were dried and prepared to meet passing criteria of 180µm. The prepared homogeneous sample is weighed and digested under heat with a hydrochloric acid and nitric acid mixture (termed 'aqua regia').

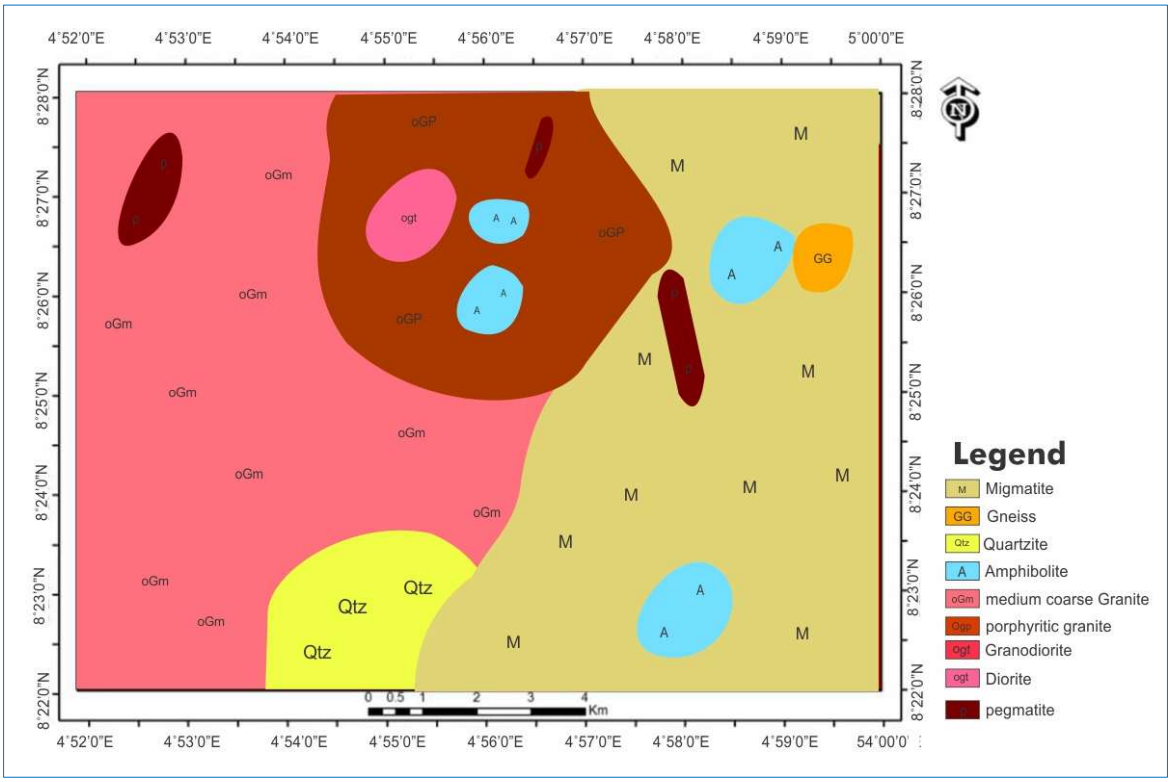

Fig. 2. Geological map of the study area

Upon completion of the digestion step, the sample is made up to volume with deionized water. This sample solution is then analyzed by Inductively Coupled Plasma-Atomic Emission Spectroscopy and Inductively Coupled Plasma Mass Spectrometry. For quality control, sample number 10 was duplicated, and a blank was prepared in the laboratory. The duplicated sample and the blank were analyzed along with the samples to serve as control. The result of the geochemical analysis was subjected to Factor Analysis and correlation using SPSS (IBM SPSS Statistic 22) and Microsoft Excel software (Office 2010), respectively. The locations of the samples analyzed are presented in Fig. 1.

3. Result Presentation and Interpretation

3.1. Local Geology of the Area

The area mapped is located within the Basement Complex of

Southwestern Nigeria. The main rock types in the study area are migmatite, banded gneiss, aplitic gneiss, quartzite, amphibolite, coarse grained biotite granite, porphyritic biotite granite, medium grained granite, fine grained granite, granodiorite, diorite, and pegmatite (Fig. 2).

Fig. 3. Field photography of a faulted section in a migmatite in the study area

Fig.4. Field photography of a granite closely associated with pegmatite in the study area

The migmatites occur in the eastern part of the area studied. It is made up of the gneisses (banded and granite gneisses) and granites (Fig. 3). The structures seen on the migmatite include, but are not limited to weak foliation, folds of different geometries, faults, and joints. The migmatite is strongly associated with porphyritic granite in the northern end, while quartzite is closely associated with it in the southern part. Like the migmatite, the gneisses dominate the western half of the area studied.

The gneisses include the banded and the granite gneisses, with subordinate aplitic gneisses. The banded gneisses are characterized with pervasive alternating bands of melanocratic and leucocratic bands while the granitic gneisses have poorly developed bands of these minerals. The aplitic gneisses in contrast to the banded gneiss have a more abundant feldspartic mineral content and are generally felsic in colour.

The amphibolites in the area studied are of two types. These are the massive and the foliated types with the massive type predominating. The massive amphibolite was encountered along the stream and river channels, while the foliated type occurs as boulders and cobbles mostly in areas of 4 m by 3 m in the northern, northeastern, and western parts of the study area.

Granites in study are fine grained and porphyritic in texture and have been extensively weathered, occurring, like the amphibolite, as boulders predominating the western half of the area. These rocks are characterized by open joints and fault planes. Petrographically, the porphyritic granite is characterized by phenocrysts of feldspar suspended within finer groundmass of alkali feldspar, plagioclase feldspar and quartz. Like the porphyritic granite, fine grain granite was also mapped in the study area. The rock is dominated by quartz and alkali feldspar. They have a characteristic sugary appearance in hand-specimen. Most of the fine-grained granites occur as veins and dykes within other granitic intrusions. Fig. 4 shows the outcrop of one of the granites that is strongly associated with a pegmatite.

Other rocks seen in the area are granodiorite (Fig. 5), pegmatite and quartzite. Unlike the pegmatites that occur as hilly exposures, especially along Agunji-Ekudaji axis, the granodiorite and the quartzite occur as intrusions within other rock types. The pegmatites are barren in most places, except for a few that have been weathered and showed indications of mineralization.

Fig. 5. Field photography of granodiorite with a quartz vein

3.2. Granulometric Analyses

Result of the grains retained in each of the sieve mesh sizes is shown in Table 1a. The granulometric analyses of results in Table 1a were used to calculate grain size parameters such as inclusive graphic mean, inclusive graphic standard deviation,

inclusive graphic skewness, and inclusive graphic kurtosis (Table 1b). From the inclusive graphic meaning, the sediments grain sizes range from exceptionally fine gravel to medium sand while the inclusive graphic standard deviation shows that most of the samples are poorly sorted (Table 1b).

Others are either very poorly sorted or moderately sorted based on the classification of Folks and Wards (1957). This implies that the sediments have not been transferred far from their source, i.e. they are mostly immature. This assertion is also confirmed by the inclusive graphic skewness, which shows that most of the sediments are negatively skewed and symmetrical. The negative skewness implies that the sediments were deposited in low-energy environment where gentle current or settling processes dominated. Unlike the negatively skewed sediments, very positively to positively skewed sediments are interpreted to depict coarse grained sediments that were deposited in a high-energy environment.

The positively skewed sediments are subordinate relative to the negatively skewed ones. These samples are platykurtic, except sample 48 which is leptokurtic. Implication of this platykurtic is that the sediments were transported through multiple mechanisms and multiple depositional events.

Table 1a. Weight of sample retained in each of the sieve mesh sizes

Sample location	Weight retained in each of the sieve mesh sizes (mm)								Cumulative weight retained
	4.5	4.0	2.0	1.0	0.5	0.25	0.125	0.63	
4	18.0	2.0	22.0	26.5	18.2	9.8	2.3	0.4	0.7
9	27.7	0	1.4	4.3	14.8	27.6	20.3	3.3	0.5
10	6.1	1.8	9.6	15.2	22.4	23.5	13.0	5.4	2.9
11	23.2	2.3	17.0	17.0	15.5	14.6	6.7	1.9	1.6
13	4.4	0.5	7.8	19.2	33.4	29.6	4.9	0.1	0.0
17	27.0	3.9	30.1	23.4	11.2	3.7	0.6	0.0	0.0
20	7.2	1.8	10.9	10.1	9.9	12.8	20.4	18.1	8.6
22	28.6	2.3	23.8	24.7	15.7	4.2	0.5	0.0	0.0
23	4.0	3.2	18.2	10.8	10.2	9.8	5.6	1.5	0.5
24	0.5	0.0	2.2	13.4	41.2	33.5	7.9	0.8	0.4
25	5.5	1.9	18.1	30.9	28.9	12.5	1.8	0.2	0.1
26	44.5	4.1	20.1	14.7	9.8	5.1	1.4	0.2	0.0
27	54	3.8	22.2	13.7	4.8	0.9	0.1	0.4	0.0
30	3.0	1.4	14.2	33.8	32.3	13.9	1.1	0.2	0.0
32	41.5	6.6	27.0	11.3	8.5	4.2	0.8	0.0	0.0
33	12.0	2.3	15.2	15.6	21.7	23.2	7.5	1.6	0.8
34	11.6	4.7	28.0	21.2	14.4	13.0	5.9	0.7	0.3
35	38.2	3.9	19.2	21.1	11.2	3.6	1.5	0.8	0.3
37	15.9	4.1	27.7	27.9	17.3	5.9	1.0	0.1	0.0
41	31.7	5.3	37.2	20.4	4.8	0.5	0.0	0.0	0.0
43	22.8	7.0	46.6	20.1	3.1	0.2	0.0	0.0	0.0
45	24.9	1.4	10.0	9.9	18.2	26.7	7.9	0.5	0.4
47	4.8	1.9	17.6	40.2	27.2	7.8	0.4	0.0	0.0
48	3.6	1.6	13.3	17.0	23.4	29.6	10.3	0.8	0.3

Table 1b. Summary of particle size parameters of the samples studied

Sample no	Sample location	Inclusive graphics mean value	Inclusive graphic standard deviation value	Inclusive graphic skewness value	Inclusive graphic kurtosis value
1	4	Very coarse sand	Poorly sorted	Nearly symmetrical	Very platykurtic
2	9	Coarse sand	Very Poorly sorted	Very pegatively skewed	Very platykurtic
3	10	Coarse sand	Poorly sorted	Negatively skewed	Very platykurtic
4	11a	Coarse sand	Very poorly sorted	Very positively skewed	Very platykurtic
5	13	Coarse sand	Poorly sorted	Negatively skewed	Very platykurtic
6	17b	Very fine gravel	Poorly sorted	Nearly symmetrical	Very platykurtic
7	20A	Medium sand	Very poorly sorted	Negatively skewed	Very platykurtic
8	22b	Very fine gravel	Poorly sorted	Nearly symmetrical	Very platykurtic
9	23	Very fine gravel	Very poorly sorted	Positively skewed	Very platykurtic
10	24A	Coarse sand	Moderately sorted	Nearly symmetrical	Very platykurtic
11	25	Very coarse sand	Poorly sorted	Nearly symmetrical	Very platykurtic
12	26a	Very fine gravel	Poorly sorted	Positively skewed	Platykurtic
13	27	Very fine gravel	Poorly sorted	Very positively skewed	Very platykurtic
14	30	Very coarse sand	Poorly sorted	Nearly symmetrical	Platykurtic
15	32b	Very fine gravel	Poorly sorted	Positively skewed	Platykurtic
16	33a	Coarse sand	Poorly sorted	Negatively skewed	Very platykurtic
17	34	Very coarse sand	Poorly sorted	Positively skewed	Very platykurtic
18	35	Very fine gravel	Poorly sorted	Positively skewed	Very platykurtic
19	37	Very coarse sand	Poorly sorted	Very pegatively skewed	Very platykurtic
20	41	Very fine gravel	Poorly sorted	Negatively skewed	Very platykurtic
21	43	Very fine gravel	Moderately sorted	Negatively skewed	Very platykurtic
22	45	Very coarse sand	Very poorly sorted	Negatively skewed	Very platykurtic
23	47	Very coarse sand	Poorly sorted	Nearly symmetrical	Very platykurtic
24	48	Coarse sand	Poorly sorted	Negatively skewed	Leptokurtic
25	49	Very coarse sand	Very poorly sorted	Positively skewed	Very platykurtic

Table 2. Result of the elemental analysis of the selected stream sediment samples

Sample no	Elements																
	Ag	Al (%)	As	Au	B	Ba	Be	Bi	Ca (%)	Cd (%)	Ce	Co	Cr	Cs	Cu	Fe (%)	Ga
4	<0.01	0.93	3.3	<0.0005	17	454	1.93	0.08	0.22	0.11	138.93	52.1	166	0.52	21	5.42	5.53
10	0.03	2.24	1.5	0.0007	12	134	0.99	0.45	0.9	0.05	52.91	19.9	65	3.74	25.2	3.63	8.7
13	<0.01	1.03	1.8	<0.0005	12	465	0.89	0.04	1.78	0.07	113.12	45.6	93	0.88	19.3	2.54	5
22	0.01	0.46	1.6	<0.0005	14	63	0.61	0.09	0.03	0.03	63.5	7.6	145	0.51	12.2	3.2	3.2
24	0.01	0.43	1.1	<0.0005	<10	78	0.31	0.02	0.06	0.05	59.03	6.2	103	0.2	8.8	2.28	2.28
25	<0.01	0.79	2	<0.0005	11	141	0.61	0.04	0.07	0.02	87.87	13.2	179	0.28	16.3	4.1	4.1
26	0.02	1.18	5.3	0.0005	18	79	2.21	0.1	0.04	0.09	249.42	17	218	0.4	28.3	8.53	8.53
27	<0.01	1.02	1.4	<0.0005	14	153	0.73	0.03	0.16	0.02	63.22	17.3	193	0.28	20.8	5.31	5.31
30	<0.01	0.41	1.1	<0.0005	11	59	0.5	0.1	0.03	0.04	51.39	6.8	114	0.53	9.6	2.44	2.44
32	<0.01	1.35	3	<0.0005	17	213	1.79	0.07	0.19	0.03	119.77	26	167	0.5	26.9	7.11	7.11
33	0.03	1.80	2.1	<0.0005	16	319	0.86	0.07	0.09	0.03	145.7	24.5	169	1.36	38.5	6.84	6.84
34	0.02	0.86	1.1	<0.0005	17	100	1.14	0.12	0.04	0.02	87.67	23.5	229	1	19.3	5.33	5.33
35	0.02	1.81	3.6	<0.0005	21	419	1.6	0.19	0.04	0.03	220.55	60.8	502	1.02	35.5	9.05	9.05
37	0.01	1.12	2.7	<0.0005	14	149	1.36	0.11	0.05	0.03	87.44	19.8	303	0.7	20.7	5.66	5.66
41	0.01	1.11	4.1	<0.0005	19	161	1.43	0.12	0.04	0.04	117.81	12.9	213	0.47	27.7	7.51	7.51
43	0.01	0.95	3	0.0005	14	106	1.13	0.57	0.04	0.03	75.73	15.3	224	0.39	22.2	5.88	5.88
45	<0.01	0.76	2.9	<0.0005	12	287	1.43	0.07	0.23	0.04	108.2	36.6	106	0.69	13.4	3.24	3.24
47	0.01	0.44	1.7	0.0006	<10	71	0.39	0.06	0.09	0.02	71.63	7	136	0.31	9.9	2.42	2.42
48	<0.01	0.64	1.3	<0.0005	<10	140	0.71	0.05	0.16	0.03	61.37	15.9	92	0.41	14.9	3.14	3.14
49	0.02	1.82	2.6	<0.0005	19	840	1.33	0.11	0.14	0.06	276.36	57.8	151	1.46	33.9	5.53	5.53

Table 2 continued

Sample no	Elements																
	Ge	Hf	Hg	In	K (%)	La	Li	Mg (%)	Mn	Mo	Na (%)	Nb	Ni	P	Pb	Rb	Re
4	0.11	0.16	0.006	0.017	0.11	14.7	5.3	0.1	2559	7.12	0.07	0.47	49.1	264	35.7	8.9	0.002
10	0.23	0.09	<0.005	0.023	0.61	22.4	10.7	1.06	660	2.81	0.13	0.62	18	1704	8.7	53.3	0.001
13	0.13	0.08	<0.005	0.012	0.26	23.2	5.2	0.53	2056	2.46	0.1	0.44	42	587	17.8	23.2	<0.001
22	0.1	0.1	0.006	0.019	0.04	20.2	2.4	0.04	425	8.78	0.02	1.38	9.9	149	10.1	5.3	0.002
24	0.07	0.07	0.008	0.013	0.06	16.3	1	0.05	413	8.67	0.03	1.09	6.7	138	13.6	5.8	0.002
25	0.1	0.08	0.009	0.017	0.1	13.1	2.3	0.06	731	18.58	0.05	0.58	12.7	143	13	8.4	0.005
26	0.24	0.17	<0.005	0.039	0.05	99.1	4	0.03	589	6.67	0.02	0.71	21.4	439	24.7	5.9	0.001
27	0.13	0.13	<0.005	0.027	0.09	10.9	2.6	0.1	851	15.72	0.07	0.93	16.1	294	10.6	7.8	0.004
30	0.1	0.1	0.005	0.015	0.05	17.3	3.1	0.03	405	7.99	0.02	0.98	8.7	113	10.3	5.7	0.002
32	0.15	0.15	0.008	0.027	0.08	15.6	4.2	0.09	1107	14.35	0.1	0.55	20.4	418	17.5	7.1	0.003
33	0.12	0.12	0.006	0.046	0.47	37.8	11.6	0.43	1190	7.46	0.06	0.68	31.2	261	19.7	26.5	0.002
34	0.13	0.13	<0.005	0.029	0.04	15.2	4.7	0.03	623	17.88	0.02	1.05	31.5	333	18.5	6.5	0.005
35	0.2	0.2	<0.005	0.044	0.16	37.1	8.3	0.19	2151	7.92	0.05	0.61	146	203	61.6	19.7	0.002
37	0.17	0.17	<0.005	0.024	0.16	9.6	6.2	0.06	593	16.4	0.05	0.56	44.9	228	25	10.7	0.003
41	0.2	0.2	<0.005	0.034	0.09	33.5	3	0.05	760	7.83	0.03	2.41	20.2	242	25.8	9.4	0.002
43	0.17	0.17	<0.005	0.024	0.06	11.9	4.2	0.03	701	16.94	0.03	0.44	17.9	236	14.6	6.4	0.004
45	0.1	0.1	<0.005	0.011	0.14	13.5	4.8	0.13	1694	5.92	0.1	0.66	26.1	364	16.7	11.4	0.001
47	0.12	0.12	<0.005	0.01	0.08	30.8	2	0.05	398	17.99	0.05	0.69	9	136	6.3	5.8	0.004
48	0.09	0.09	<0.005	0.014	0.08	10.2	2.9	0.09	718	7.56	0.06	0.65	12.7	326	9.9	6.2	0.002
49	0.19	0.19	0.006	0.04	0.29	50.8	14.1	0.3	3812	13.38	0.09	1.24	36.8	138	37.6	25.1	0.003

Table 2 continued

Sample no	Elements																
	S (%)	Sb	Sc	Se	Sn	Sr	Ta	Te	Th	Ti (%)	Tl	U	V	W	Y	Zn	Zr
4	<0.01	0.2	2.8	<0.2	0.5	15.5	<0.01	0.08	3.2	0.05	0.21	1.71	149	0.14	6.28	42	5.9
10	<0.01	0.13	8.3	<0.2	0.9	47.3	<0.01	<0.01	2.5	0.287	0.34	0.61	87	0.16	12.35	57	2.9
13	<0.01	0.09	3.7	<0.2	0.4	54.1	<0.01	<0.01	2.6	0.102	0.25	0.6	86	0.15	9.98	30	2.7
22	<0.01	0.14	2.8	<0.2	0.4	4.3	<0.01	0.02	10.2	0.139	0.05	0.98	70	0.52	3.12	16	4.2
24	<0.01	0.13	1.6	<0.2	0.3	7.8	<0.01	<0.01	6.6	0.171	0.05	0.29	51	0.08	2.37	27	3.4
25	<0.01	0.22	2.4	<0.2	0.4	10.9	<0.01	0.06	5.2	0.073	0.07	0.42	82	0.11	3.12	15	3.6
26	<0.01	0.33	5.9	<0.2	0.7	5.3	<0.01	0.06	48.4	0.127	0.07	3.12	199	0.49	11.01	45	7.8
27	<0.01	0.22	4.2	<0.2	0.8	20.4	<0.01	<0.01	4.4	0.235	0.09	0.56	133	0.1	3.96	18	5.7
30	<0.01	0.11	2.1	<0.2	0.4	5	<0.01	<0.01	7.5	0.182	0.05	0.79	50	0.13	2.91	19	4.1
32	<0.01	0.37	3.9	<0.2	0.7	31.5	<0.01	0.02	4.8	0.147	0.1	0.88	192	0.11	5.77	22	6.3
33	<0.01	0.19	9.1	<0.2	1	11.3	<0.01	0.11	13.5	0.199	0.17	1.02	167	0.08	8.87	44	5.6
34	<0.01	0.22	3.6	<0.2	0.9	4.8	<0.01	0.02	5.9	0.147	0.1	0.98	95	0.17	4.88	19	6.8
35	<0.01	0.24	6.4	0.2	0.8	9.5	0.01	0.14	16.2	0.101	0.28	2.16	198	0.28	7.64	26	9.8
37	<0.01	0.21	2.9	<0.2	0.7	14.6	<0.01	0.05	3.8	0.057	0.11	1.49	121	0.14	4.24	14	7.4
41	<0.01	0.29	3.9	<0.2	0.8	6	0.02	0.06	21	0.112	0.1	6.38	175	0.51	14.42	23	9.8
43	<0.01	0.28	3.4	<0.2	0.7	5.8	<0.01	0.08	5.4	0.064	0.07	1.34	122	0.22	3.96	15	7.3
45	<0.01	0.16	2.2	<0.2	0.5	25.6	<0.01	0.02	2.8	0.041	0.23	1.04	91	0.09	5.88	12	3.7
47	<0.01	0.14	1.6	<0.2	0.6	13.5	<0.01	<0.01	13.3	0.161	0.05	0.99	39	0.12	5.05	10	5.8
48	<0.01	0.18	2.3	<0.2	0.5	19.3	<0.01	0.01	3.5	0.124	0.06	0.45	82	0.07	3.97	15	4
49	<0.01	0.15	8.4	<0.2	0.9	9.2	<0.01	<0.01	19	0.268	0.45	1.74	113	0.86	15.13	31	8.9

3.3. Geochemical Analysis

The result of the geochemical analysis is presented in Table 2, with a total of 51 elements consisting of trace and rare-earth elements. From Table 2, S and Ta have a constant value <0.01 ppm and 0.01 ppm in all the samples analyzed. These are like the concentration of Se with a value of 0.19 ppm except location 35 (Longitude 4.932˚E, Latitude 8.398˚N) with a concentration of 0.2 ppm.

Au has its highest concentration value (0.007 ppm) in the sample from location 10 (Longitude 4.92˚E and Latitude 8.45˚N). The highest concentration values of these metals Ag (0.03 ppm), Al (2.24 ppm), Cs (3.74 ppm), K (0.61 ppm), Mg (1.06 ppm), Na (0.13 ppm), P (1704 ppm), Rb (53.3 ppm), Ti (0.287 ppm) and Zn (57 ppm) were also recorded in this location. This location has the second highest concentration of other ore-forming or pathfinder elements such as Bi, Sn, Sr, Tl etc.

Like location 10, location 41 (Longitude 4.93˚E, Latitude 8.42˚N) has the highest concentration of Arsenic (As) (4.1 ppm). Other elements with the highest concentration recorded in this location include B (19 ppm), Hf (0.2 ppm), Nb (2.41 ppm), Ta (0.02 ppm), U (6.38 ppm) and Zr (9.8 ppm). Location 30 (Longitude 4.99˚E, Latitude 8.46˚N) has the lowest or almost lowest concentration for most of the analyzed elements.

3.4. Heavy Minerals Composition and Characteristics

The result of heavy mineral analysis is presented in Figs. 6–10. The identified heavy minerals include apatite, epidote, garnet, hematite, ilmenite, olivine, rutile, sillimanite, topaz, zoisite, hypersthene, zircon, corundum, and goethite. These minerals are angular to sub-round shape indicating that some of them have been transported far from their source(s), while some of them have not been transported far from their source(s).

Few heavy minerals, however, occur as angular grains, suggesting proximity to their source(s). Hematite and goethite are seen and described as opaque minerals under transmitted light microscope, but hematite appears grey while the goethite is reddish-brown under reflected microscope. Rutile and tourmaline in some samples are products of alteration and occur as gangue minerals (Stendal and Theobald, 1994).

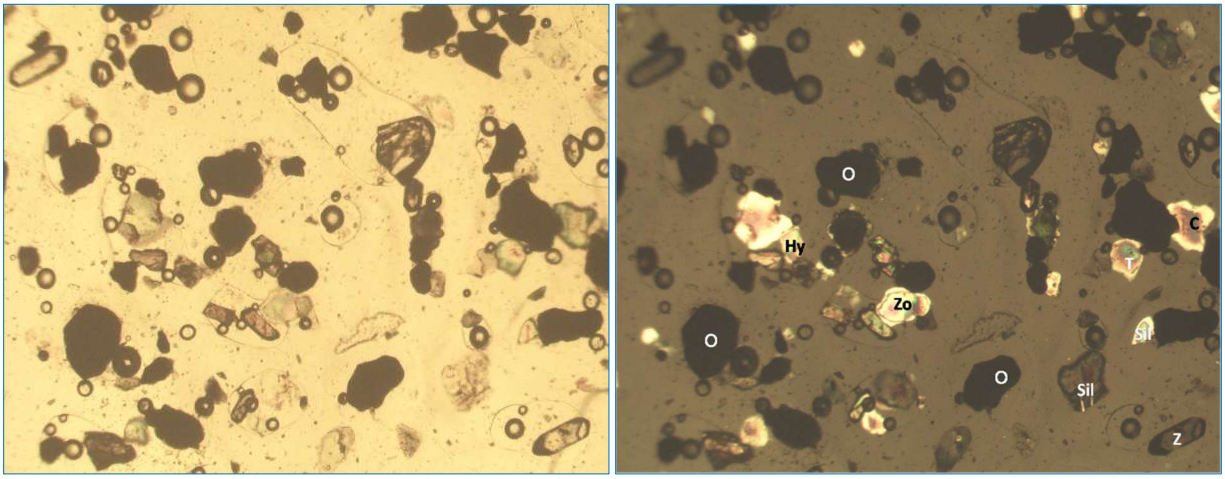

L4 – Z: Zircon, Sil: Sillimanite, Zo: Zoisite, Hy: Hypersthene, C: Corundum, T: Topaz, O: Opaque (goethite and hematite). Left – PPL and Right – XPL

Fig. 6. Photomicrograph of heavy minerals in location 4

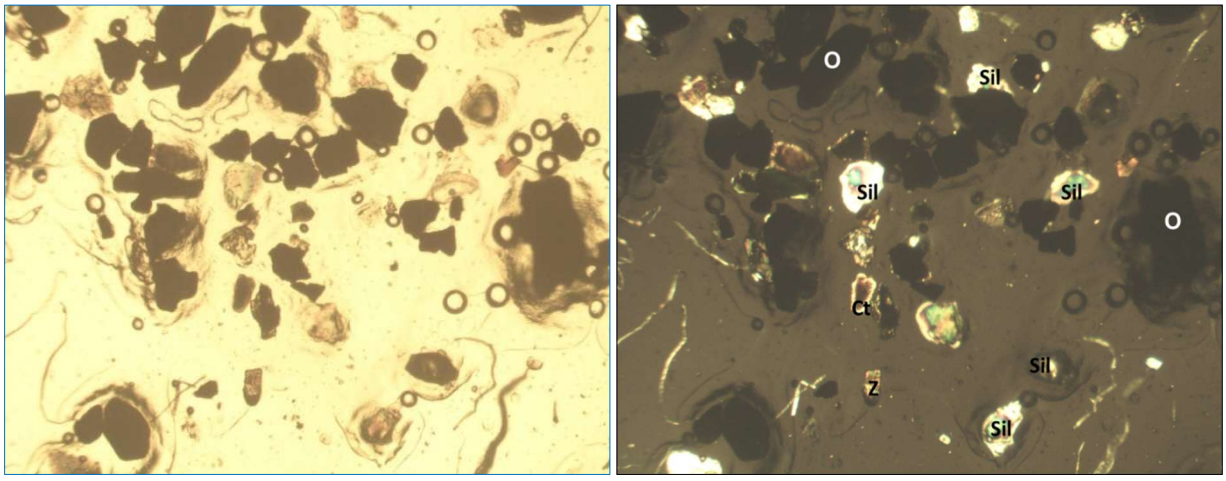

L10 – Sil: Sillimanite, Z: Zircon, Ct: Cassiterite, O: Opaque (goethite and hematite). Left – PPL and Right – XPL

Fig. 7. Photomicrograph of heavy minerals in location 10

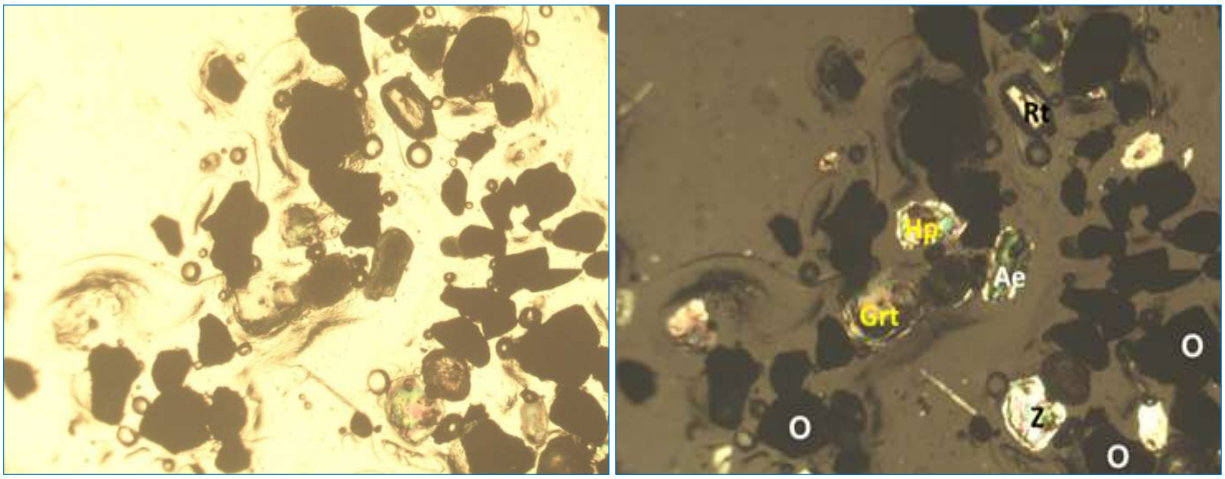

L13 – Ae: Aegirine, Hp: Hypersthene, Grt: Garnet, Rt: Rutile, O: Opaque (goethite and hematite). Left – PPL and Right – XPL

Fig. 8. Photomicrograph of heavy minerals in location 13

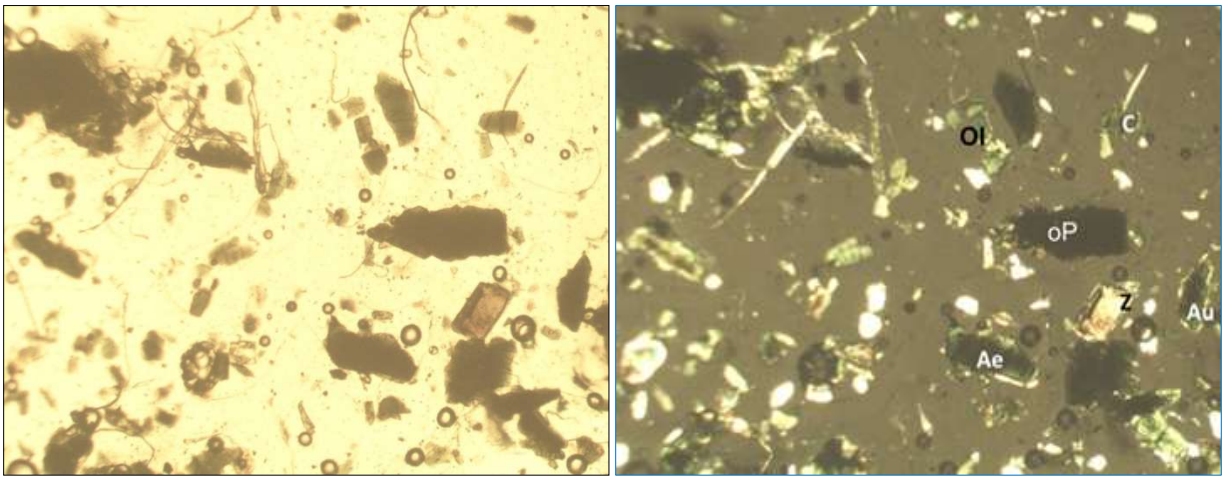

L27 – Ol: Olivine, Z: Zircon, C: Chloritoid, Au: Augite, Ae: Aegirine, Op: Opaque (goethite and hematite). Left – PPL and Right – XPL

Fig. 9. Photomicrograph of heavy minerals in location 27

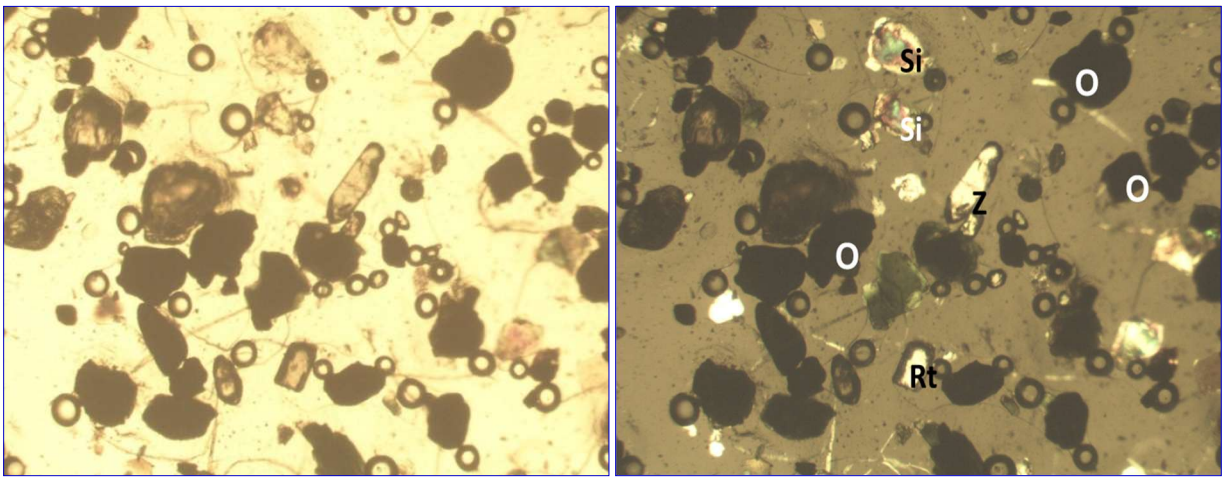

L45 – Rt: Rutile, Si: Sillimanite, Z: Zircon, O: Opaque (goethite and hematite). Left – PPL and Right – XPL

Fig. 10. Photomicrograph of heavy minerals in location 45

Furthermore, most of the heavy minerals are subhedral to anhedral, indicating that the heavy minerals have been through short to long transportation from their source. Few of the heavy minerals are euhedral, suggesting proximity to their source(s). Sample from location 4 is relatively rich in heavy minerals compared to other locations such as 9, 17, 26, 34, 35 and 41 with sillimanite, zircon and iron ore only. Other locations that are enriched in heavy minerals are

locations 10 and 20. The presence of sillimanite in the samples analyzed is an indication of the presence of sulphide mineralization, which may be Cu-Zn ± Pb-Ag-Au (Spry et al., 2022, Berke et al., 2023; McClenaghan et al., 2023). This mineral is also associated with gneisses, which can be ortho- or paragneisses.

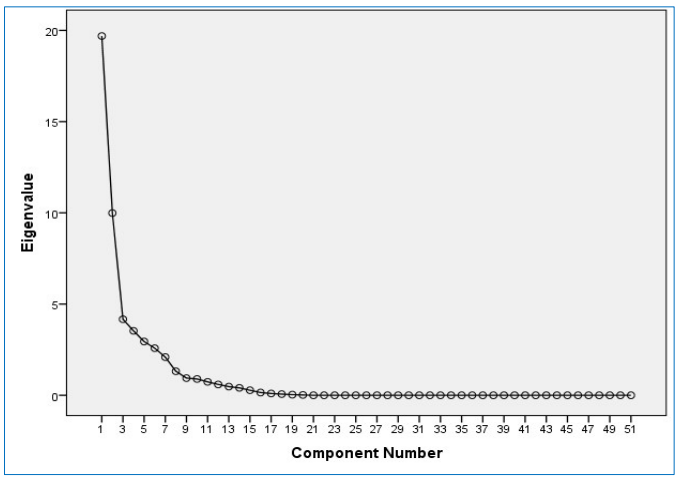

Fig. 11. Scree plot of the principal components

Similarly, Ghosh and Praveen (2008) opined that sulphide mineralization hosted by felsic rock has staurolite, spinel, biotite, and ilmenite as associated indicator minerals. These minerals occur within the foot-wall alteration zones in proximity to sulphide mineralization. The presence of some of these minerals is equally interpreted as an indication of sulphide ore mineralization within the study area. Topaz is found in felsic igneous rocks and is commonly associated with some hydrothermal vein deposits and hydrothermally altered rocks (Stendal and Theobald 1994). Topaz indicates the presence of Ta-Na-W mineralization along with gangue minerals that include arsenopyrite, quartz, fluorite and loellingite (McClenaghan et al., 2015).

Tourmaline has many species and is associated with rocks of varying petrogenetic affinities. The characteristics of this mineral make them not only good indicator of mineralization alone but also as dependable geothermometer and geobarometer indicator (Chapman et al., 2015). It usually indicates the presence of hydrothermal metallic mineral deposits. Zoisite is diagnostic of hydrothermal assemblages, and it is associated with gold mineralization (Roache et al., 2011).

3.5. Principal Component Analyses

The result of the Principal Component Analysis (PCA) is shown in Tables 3 and 4 while Fig. 11 shows the scree plot for the PCA. The rotated component matrix culminated in 8 distinct Factor Groups. Factor 1 has Fe, V, Sb, Cr, Be, Te, Hf, B, Zr, Cu, Ga, In, Pb, Ni and Ce. Factor 2 is made up of K, Rb, Cs, Mg, Ag, Sc, Al, P, Li, Ge, Ti, Zn, Au, Sn, Na and Y. Factor 3 has Mn, Ba, Co and Tl, while Factor 4 has Th, La, W and Sr.

Furthermore, Re, Mo, Cd and Ca made up Factor 5. Factor 6 is composed of Ta, Nb and U and Factor 7 has Se and S, while Factor 8 has Hg and Bi. Each of these Factor groups has the following percentage contributions to the geological processes from Factor 1–8 respectively: 24.252, 23.396, 11.932, 6.097, 4.090, 3.783, 3.250, 3.105 and 1.688. From the scree plot (Fig. 11); the first 3 components are very significant, while the next 6 components have almost the same level of contribution to the geological processes in the area. Components 10 to 51 contributions are minimal in the overall geological processes but are significant in the mineralization processes.

Factor 1 is interpreted to be related to complex hydrothermal sulfide ore that are likely present in the study area, while factor 2 is related to gold-associated gangue minerals in the area that are generally described as miscellaneous by Levinson (1981). Factor 2 is also considered to be a distinct phase that is more associated with mineralization in Factor 1 during the crystallization of the mafic rocks in the area studied. Factor 3 is interpreted to imply Ba-Ag and vein deposits of mafic composition (Landergren, 1943; Ottesen and Theobald, 1994). The geochemical association in this factor group can also be interpreted as an indication of lithium-rich pegmatites, granitic dykes and coarse grained granites where lithium is accompanied by Na, K, Al etc. (Boyle, 1974), while Factor 4 is related to rare-earth granitic rocks such as granite, pegmatite and gneisses that are found in the study area (Bamigboye and Adekeye, 2011; Levinson, 1981). Factor 5 is related to copper-bearing minerals or porphyry copper related deposits and their allied (Levinson, 1981; Boyle, 1974). It is noteworthy that, unlike the previous Factor Groups, this Factor Group has both positive and negative loading of its component. Re and Mo have loadings of -0.863 and -0.850, respectively indicating that the mineralization is influenced by exogenetic material. Factor 6 is related to pegmatite with tantalite-niobium-columbite mineralization (Goldschmidt, 1954; Landergren, 1943; Levinson, 1981; Ottesen and Theobald, 1994) while Factor 7 have negative loading of its components (Se and S) which is interpreted to indicate the presence of another phase of hydrothermal sulphide mineralization in the area, but the precursor materials for the mineralization are inferred to be of differing origin. Factor 8 shows that there are protores of low temperature sulfide deposits with the possibility of associated radioactive elements (Levinson, 1981).

3.6. Isograde Plots

From the isograde plots (Figs. 12–31), Ag has its peak concentration in the southern part of the area and in the northern part. These positive anomalies are flanked by inconspicuous negative anomalies. Its geochemical relief is 0.02 ppm. The negative anomalies are aligned in SW-NE and NW-SE directions. Unlike Ag, Al positive anomalies are concentrated in the southern half of the study area, except for two negative anomalies at the southwestern end of the area. The most obvious negative anomaly is at the northwestern end of the area. Its geochemical relief is 1.7ppm. Similarly, the most obvious positive anomaly of Arsenic (As) is at the eastern end. Other areas of positive anomalies are the central part of the study area. Its geochemical relief is 4.0ppm. Au is anomalously concentrated in the SE part of the area. The other area has a uniform concentration (0.00051) described as a regional background.

The positive anomaly has a value of 0.00089 and it is flanked to the right by a negative anomaly. Unlike Au, the anomalous zones of Boron trend in E-W direction. These anomalies are characterized by alternating positive and negative anomaly. Its highest anomaly is in the western part. Ba has a different distribution pattern.

Table 3. Total variance explained

Component	Initial Eigenvalues			Extraction Sums of Squared Loadings			Rotation Sums of Squared Loadings		
	Total	% of variance	Cumulative %	Total	% of variance	Cumulative %	Total	% of variance	Cumulative %
1	19.692	38.613	38.613	19.692	38.613	38.613	12.369	24.252	24.252
2	9.989	19.587	58.199	9.989	19.587	58.199	11.932	23.396	47.649
3	4.169	8.174	66.373	4.169	8.174	66.373	6.097	11.955	59.604
4	3.530	6.921	73.294	3.530	6.921	73.294	4.090	8.019	67.622
5	2.946	5.776	79.070	2.946	5.776	79.070	3.783	7.418	75.040
6	2.581	5.060	84.131	2.581	5.060	84.131	3.250	6.372	81.412
7	2.091	4.100	88.231	2.091	4.100	88.231	3.105	6.089	87.501
8	1.316	2.580	90.811	1.316	2.580	90.811	1.688	3.310	90.811
9	0.942	1.847	92.658						
10	0.894	1.752	94.410						
11	0.736	1.442	95.852						
12	0.593	1.164	97.016						
13	0.476	0.933	97.949						
14	0.408	0.800	98.749						
15	0.276	0.540	99.289						
16	0.150	0.294	99.583						
17	0.098	0.193	99.776						
18	0.063	0.123	99.899						
19	0.034	0.067	99.966						
20	0.017	0.034	100.000						
21	1.931E-15	3.787E-15	100.000						
22	1.093E-15	2.142E-15	100.000						
23	9.320E-16	1.827E-15	100.000						
24	8.075E-16	1.583E-15	100.000						
25	7.212E-16	1.414E-15	100.000						
26	6.542E-16	1.283E-15	100.000						
27	4.988E-16	9.779E-16	100.000						
28	4.130E-16	8.098E-16	100.000						
29	3.605E-16	7.068E-16	100.000						
30	3.153E-16	6.181E-16	100.000						
31	2.607E-16	5.112E-16	100.000						
32	1.310E-16	2.568E-16	100.000						
33	1.189E-16	2.331E-16	100.000						
34	4.397E-17	8.621E-17	100.000						
35	2.323E-17	4.555E-17	100.000						
36	-5.112E-17	-1.002E-16	100.000						
37	-1.308E-16	-2.565E-16	100.000						
38	-1.650E-16	-3.235E-16	100.000						
39	-1.708E-16	-3.349E-16	100.000						
40	-3.377E-16	-6.621E-16	100.000						
41	-3.690E-16	-7.234E-16	100.000						
42	-3.869E-16	-7.585E-16	100.000						
43	-4.326E-16	-8.483E-16	100.000						
44	-5.370E-16	-1.053E-15	100.000						
45	-6.468E-16	-1.268E-15	100.000						
46	-7.310E-16	-1.433E-15	100.000						
47	-9.082E-16	-1.781E-15	100.000						
48	-1.075E-15	-2.107E-15	100.000						
49	-1.147E-15	-2.249E-15	100.000						
50	-1.498E-15	-2.938E-15	100.000						
51	-5.268E-15	-1.033E-14	100.000						

Its anomalous area is at the extreme SE corner and decreases towards the extreme NW corner in all sweeping manner. The lowest point is in the eastern part of the area.

Beryllium (Be) has an almost similar distribution pattern to B. Its positive and negative anomalies are similarly positioned. Its highest concentration is in the extreme western part, and it is strongly associated with the highest negative anomaly. Bismuth has one of its anomalies in a position like that of Au. The most obvious anomaly is in the northern part of the area. Between these two anomalies, there are 3 closely associated negative anomalies. Its regional background value is 0.14, while local aureole is 0.3 and the aureole value is 0.54.

Ca and Au distribution patterns are almost identical. Their lowest concentration is slightly below the regional background with inconspicuous negative anomalies in the western part. Their local aureole value is 1.5, while their anomalous value is 1.7. Cd have two anomalous points. Each of these points is located at the eastern and western part of the study area showing a E-W trend.

In the western part, the anomalous zone is associated with two negative anomalies that are positioned to the north and south of the anomaly. The point of negative anomaly in the east coincides with the positive anomaly of Au. The value of the regional, local and anomaly are 0.04, 0.095 and 0.105 respectively.

Table 4. Rotated component matrix

Elements	Component							
	1	2	3	4	5	6	7	8
Fe	0.945	0.158	0.080	0.184	-0.114	0.130	0.040	-0.043
V	0.933	0.164	0.105	0.089	0.077	0.112	0.109	-0.140
Sb	0.856	-0.096	-0.214	0.049	-0.145	0.085	0.301	-0.098
As	0.821	-0.070	0.130	0.285	0.259	0.150	0.238	0.117
Cr	0.809	-0.076	0.176	-0.021	-0.313	-0.012	-0.226	0.173
Be	0.802	0.040	0.267	0.149	0.245	-0.004	0.287	0.120
Te	0.789	0.038	0.054	0.007	0.006	-0.098	-0.392	-0.019
Hf	0.786	0.016	0.306	0.203	-0.236	0.278	0.151	0.241
B	0.774	0.126	0.354	0.256	-0.071	0.272	-0.108	0.001
Zr	0.759	-0.015	0.253	0.264	-0.338	0.339	0.056	0.186
Cu	0.733	0.534	0.292	0.161	-0.086	0.123	0.015	-0.125
Ga	0.723	0.616	0.241	0.134	0.000	0.061	0.053	-0.066
In	0.712	0.418	0.148	0.374	-0.228	0.187	-0.163	-0.134
Pb	0.697	0.037	0.612	0.100	0.017	0.053	-0.216	0.064
Ni	0.613	0.099	0.517	-0.146	0.027	-0.124	-0.395	0.167
Ce	0.583	0.152	0.562	0.525	0.066	0.017	0.047	-0.089
K	-0.008	0.939	0.166	-0.081	0.131	-0.036	-0.009	-0.033
Rb	0.012	0.938	0.224	-0.100	0.155	-0.001	0.016	0.110
Cs	-0.034	0.929	0.135	-0.034	0.056	-0.003	0.031	0.228
Mg	-0.125	0.914	0.130	-0.166	0.275	-0.054	0.063	0.092
Ag	0.218	0.848	-0.002	0.323	-0.024	-0.111	-0.237	-0.015
Sc	0.397	0.813	0.244	0.299	-0.057	0.046	-0.036	-0.082
Al	0.517	0.799	0.279	0.018	-0.021	0.030	0.035	-0.001
P	-0.007	0.784	-0.158	-0.197	0.321	-0.075	0.287	0.267
Li	0.249	0.743	0.521	0.165	-0.104	-0.036	-0.063	0.016
Ge	0.434	0.716	0.209	0.443	0.030	0.121	0.007	-0.075
Ti	-0.169	0.706	0.045	0.295	-0.313	0.145	0.246	-0.125
Zn	0.307	0.700	0.085	0.278	0.365	-0.078	0.214	-0.082
Au	-0.245	0.686	-0.239	-0.089	0.059	-0.054	0.157	0.399
Sn	0.540	0.628	0.081	0.133	-0.379	0.185	0.052	0.104
Na	-0.005	0.593	0.412	-0.394	0.200	-0.121	0.385	-0.072
Y	0.323	0.568	0.365	0.291	0.232	0.459	0.208	0.080
Mn	0.212	0.171	0.935	0.063	0.066	0.000	0.079	-0.077
Ba	0.166	0.247	0.925	0.071	0.041	0.041	0.032	-0.138
Co	0.402	0.198	0.860	-0.078	0.132	-0.122	-0.012	0.028
Tl	0.103	0.609	0.748	0.003	0.113	0.025	0.015	0.115
Th	0.453	0.010	-0.072	0.815	0.153	0.177	0.053	0.020
La	0.410	0.199	0.065	0.802	0.224	0.056	0.110	0.005
W	0.158	0.083	0.414	0.620	-0.087	0.463	0.078	0.131
Sr	-0.099	0.499	0.185	-0.502	0.400	-0.142	0.420	0.011
Re	0.111	-0.175	-0.063	-0.130	-0.863	-0.074	0.209	-0.061
Mo	0.223	-0.204	-0.043	-0.044	-0.850	-0.086	0.344	-0.016
Cd	0.210	0.040	0.370	0.336	0.600	-0.098	0.403	0.051
Ca	-0.223	0.398	0.274	-0.334	0.501	-0.072	0.285	0.077
Ta	0.239	-0.088	-0.132	-0.078	0.156	0.915	-0.103	0.049
Nb	0.072	-0.007	-0.006	0.224	-0.183	0.881	0.174	-0.060
U	0.556	-0.078	0.003	0.237	0.171	0.736	0.041	0.174
Se	0.071	-0.126	0.091	-0.091	0.160	-0.109	-0.883	0.131
S	-0.394	-0.207	-0.161	-0.011	0.245	-0.046	-0.655	0.012
Hg	0.016	-0.089	-0.034	-0.104	-0.151	-0.150	0.204	-0.736
Bi	0.237	0.416	-0.160	-0.098	-0.131	-0.085	0.071	0.633

Distribution pattern of Ce is like that of Be and B. Its anomalous positions are in SE-NW direction with associated negative anomalies. Its geochemical relief is 210. It was also observed that the southern part of the study area is more enriched than the northern part. Co has 3 anomalous points in the area investigated. Its peak is in the western part defined by Long. 8.4˚ and Latitude 4.93˚. Its geochemical relief is 50. Other elements with similar or identical distribution patterns to Au, Ca and Bi are Cd, Ca, Cr, Cs, K, La, Mg, Mn, Nb, Ni, Rb, Zn, P, Pb, Se, Sr, Ta, and U. These elements have their anomalous point similarly or identically positioned positive and negative anomalies. Similarly, the distribution patterns of Cu, Fe, Ga, Ge, Hf, In, Li, Mo, Na, Te, Th, Tl, V, W, Y, Zr are the same or like those of Be, Ba, B, As, Al. Other elements with distribution patterns that are different from these two, like Ag are Hg, Re, Sb, Ti. Oraphan et al. (2023) predicted that Ag, As and Cu are elements that indicate Au mineralization.

While Figs. 12–19 affirm that the southeastern part of the area is mineralized, Figs. 20–29 show mineralization in the western part of the area. The elements with their peaks in the southeastern part indicate mineralization of precious metals while those with their peaks in the western part show possible mineralization of rare-earth metals that are hosted by pegmatites in the northwestern part of the area.

Arsenic, a moderate siderophile element, has an exceptionally positive correlation with Be, Ce, Fe, Cu, Ga, Hf, In, La, Pb, Te, Th, U, V and Zr (Table 5).

Table 5. Correlation table for selected element

	As	Au	Be	Bi	Ca	Cd	Ce	Co	Cr	Cs	Cu	Fe	Ga	Ge	Hf	In	K	La	Li	Mg	Mn	Mo	Na	Nb	Ni	P	Pb	Sr	Te	Th	Ti	Tl	U	V	W	Y	Zn	Zr
As	1																																				
Au	-0.23	1																																			
Be	0.55	-0.19	1																																		
Bi	0.13	0.45	0.13	1																																	
Ca	-0.18	0.32	-0.06	0.07	1																																
Cd	0.45	-0.03	0.32	-0.04	0.32	1																															
Ce	0.69	-0.26	0.67	-0.09	-0.08	0.46	1																														
Co	0.32	-0.16	0.54	-0.02	0.43	0.43	0.67	1																													
Cr	0.47	-0.30	0.42	0.13	-0.37	-0.18	0.43	0.35	1																												
Cs	-0.14	0.74	0.06	0.49	0.41	0.10	0.10	0.26	-0.15	1																											
Cu	0.54	-0.04	0.58	0.23	0.000	0.15	0.72	0.55	0.49	0.40	1																										
Fe	0.77	-0.27	0.75	0.17	-0.33	0.11	0.66	0.55	0.73	0.004	0.83	1																									
Ga	0.54	0.13	0.63	0.28	0.07	0.20	0.69	0.54	0.46	0.54	0.96	0.80	1																								
Ge	0.43	0.26	0.42	0.20	0.09	0.23	0.71	0.38	0.17	0.60	0.86	0.58	0.87	1																							
Hf	0.74	-0.24	0.70	0.24	-0.37	0.16	0.65	0.41	0.69	-0.05	0.66	0.83	0.59	0.43	1																						
In	0.50	-0.16	0.49	0.15	-0.28	0.01	0.70	0.34	0.59	0.26	0.91	0.86	0.86	0.81	0.67	1																					
K	-0.12	0.60	-0.02	0.32	0.48	0.11	0.13	0.29	-0.19	0.88	0.50	0.01	0.57	0.67	-0.12	0.29	1																				
La	0.64	0.001	0.47	-0.05	-0.07	0.45	0.77	0.15	0.19	0.09	0.49	0.51	0.51	0.71	0.41	0.58	0.10	1																			
Li	0.13	0.25	0.30	0.29	0.19	0.18	0.568	0.62	0.14	0.74	0.75	0.33	0.75	0.80	0.33	0.61	0.79	0.29	1																		
Mg	-0.18	0.71	-0.05	0.36	0.68	0.18	0.02	0.27	-0.29	0.91	0.35	-0.12	0.47	0.54	-0.24	0.11	0.93	0.05	0.64	1																	
Mn	0.26	-0.20	0.42	-0.09	0.25	0.46	0.69	0.92	0.13	0.22	0.49	0.22	0.44	0.40	0.38	0.29	0.28	0.18	0.64	0.22	1																
Mo	-0.14	-0.17	-0.16	0.004	-0.51	-0.56	-0.14	-0.26	0.27	-0.37	-0.12	0.08	-0.21	-0.26	0.21	0.01	-0.42	-0.25	-0.22	-0.52	-0.20	1															
Na	-0.08	0.45	0.16	0.09	0.62	0.17	0.07	0.48	-0.33	0.59	0.24	-0.13	0.35	0.30	-0.16	-0.10	0.66	-0.17	0.50	0.72	0.48	-0.31	1														
Nb	0.08	-0.14	-0.09	-0.16	-0.28	-0.11	0.02	-0.25	-0.02	-0.09	0.03	0.10	0.04	0.08	0.25	0.22	-0.18	0.14	-0.13	-0.21	-0.10	-0.05	-0.37	1													
Ni	0.36	-0.15	0.44	0.08	0.05	0.10	0.53	0.75	0.81	0.14	0.53	0.54	0.55	0.28	0.51	0.47	0.13	0.15	0.41	0.10	0.51	-0.16	0.09	-0.20	1												
P	-0.07	0.79	0.12	0.49	0.58	0.19	-0.15	0.04	-0.30	0.83	0.17	-0.08	0.37	0.36	-0.23	-0.02	0.70	0.03	0.35	0.86	-0.07	-0.46	0.63	-0.21	-0.06	1											
Pb	0.58	-0.30	0.62	0.01	-0.12	0.32	0.76	0.79	0.76	0.07	0.65	0.68	0.62	0.40	0.72	0.61	0.05	0.34	0.47	-0.04	0.67	-0.14	0.01	0.02	0.90	-0.20	1										
Sr	-0.18	0.46	0.02	0.08	0.68	0.17	-0.18	0.27	-0.39	0.48	0.02	-0.28	0.15	0.08	-0.38	-0.31	0.54	-0.22	0.20	0.72	0.18	-0.43	0.85	-0.41	0.01	0.71	-0.20	1									
Te	0.56	-0.25	0.43	0.23	-0.28	0.08	0.43	0.35	0.73	-0.05	0.62	0.71	0.54	0.34	0.54	0.60	0.10	0.24	0.28	-0.08	0.18	-0.04	-0.24	-0.14	0.67	-0.20	0.67	-0.34	1								
Th	0.68	-0.12	0.45	-0.07	-0.28	0.34	0.69	-0.01	0.27	-0.10	0.41	0.56	0.40	0.57	0.48	0.58	-0.11	0.96	0.10	-0.18	0.02	-0.13	-0.38	0.29	0.10	-0.13	-0.13	-0.42	0.28	1							
Ti	-0.40	0.49	-0.32	0.07	0.10	-0.10	0.04	-0.10	-0.31	0.57	0.22	-0.11	0.28	0.50	-0.13	0.28	0.51	0.20	0.43	0.52	0.04	-0.08	0.26	0.22	-0.23	0.39	-0.20	0.14	0.10	1							
Tl	0.14	0.28	0.32	0.21	0.43	0.35	0.55	0.81	0.05	0.71	0.55	0.15	0.60	0.61	0.24	0.33	0.69	0.19	0.85	0.67	0.82	-0.36	0.69	-0.10	0.48	0.42	0.53	0.42	0.09	-0.03	0.32	1					
U	0.72	-0.15	0.51	0.06	-0.22	0.23	0.41	0.07	0.36	-0.10	0.41	0.60	0.36	0.34	0.70	0.47	-0.13	0.46	0.03	-0.19	0.08	-0.15	-0.28	0.67	0.18	-0.12	0.42	-0.32	0.37	0.59	-0.18	1					
V	0.79	-0.28	0.81	0.08	-0.17	0.24	0.63	0.41	0.60	-0.004	0.82	0.95	0.81	0.56	0.74	0.77	0.07	0.46	0.31	-0.04	0.28	-0.10	0.05	0.03	0.50	0.01	0.63	-0.08	0.66	0.48	-0.14	0.56	1				
W	0.43	-0.12	0.32	0.08	-0.15	0.26	0.65	0.26	0.15	0.13	0.40	0.34	0.35	0.50	0.55	0.49	0.002	0.59	0.37	-0.03	0.43	-0.05	-0.14	0.554	0.10	-0.13	0.40	-0.33	0.02	0.61	0.24	0.39	0.24	1			
Y	0.49	0.26	0.46	0.17	0.33	0.42	0.64	0.45	0.01	0.55	0.68	0.42	0.69	0.81	0.46	0.55	0.56	0.60	0.65	0.53	0.51	-0.41	0.38	0.3	0.21	0.40	0.40	0.25	0.12	0.49	0.35	0.68	0.44	0.63	1		
Zn	0.25	0.41	0.36	0.23	0.34	0.64	0.39	0.30	-0.12	0.66	0.55	0.29	0.65	0.70	0.07	0.42	0.69	0.49	0.58	0.69	0.27	-0.59	0.35	-0.11	0.15	0.63	0.24	0.31	0.23	0.32	0.42	0.50	0.37	0.16	0.61	1	
Zr	0.66	-0.28	0.58	0.15	-0.47	0.01	0.64	0.32	0.74	-0.11	0.63	0.82	0.55	0.43	0.97	0.74	-0.18	0.44	0.28	-0.32	0.29	0.29	-0.30	0.35	0.50	0.33	0.70	-0.50	0.53	0.54	-0.08	0.71	0.68	0.56	0.42	-0.02	1

This is justified by their loading in the PCA where most of them are loaded in Factor 1, because all these elements except V, which is slightly siderophile, are non-siderophile (Table 4). This can therefore be interpreted to be enhanced by the mineralization process.

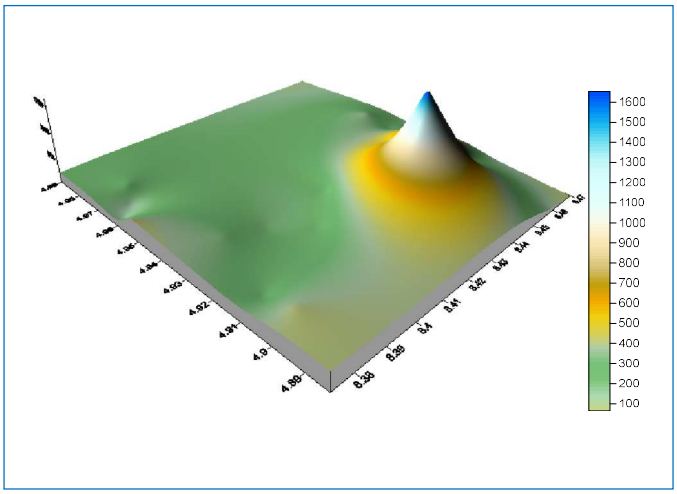

Fig. 12. Isograde plot of P distribution

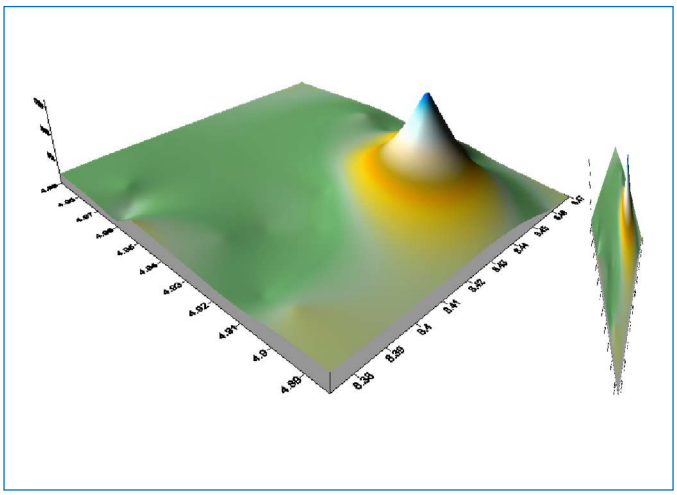

Fig. 13. Isograde plot of P distribution

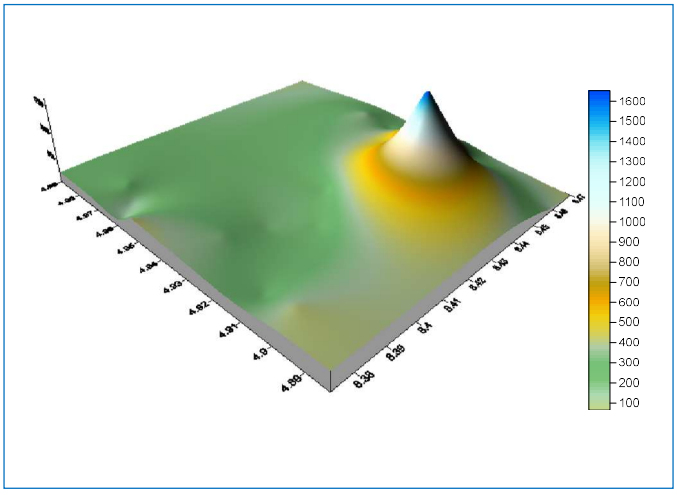

Fig. 14. Isograde plot of P distribution

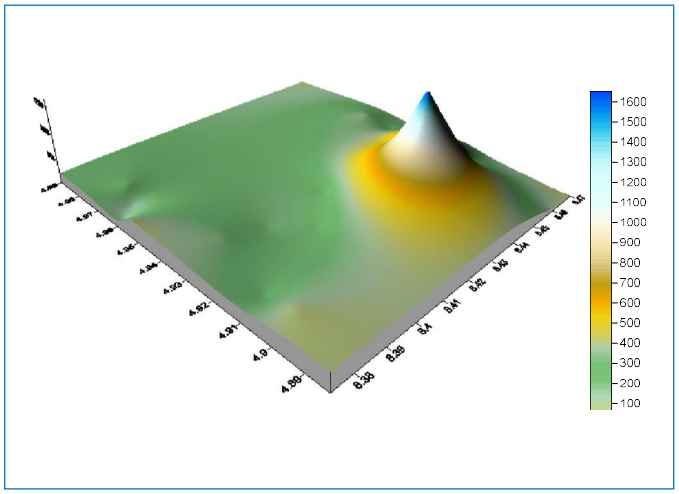

Fig. 15. Isograde plot of P distribution

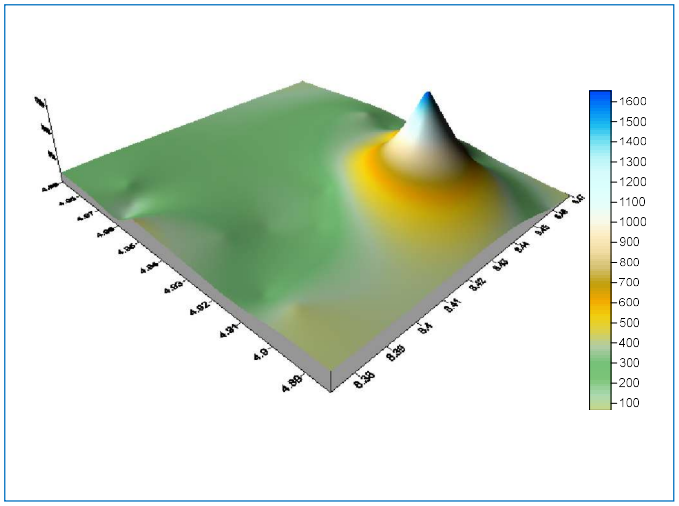

Fig. 16. Isograde plot of P distribution

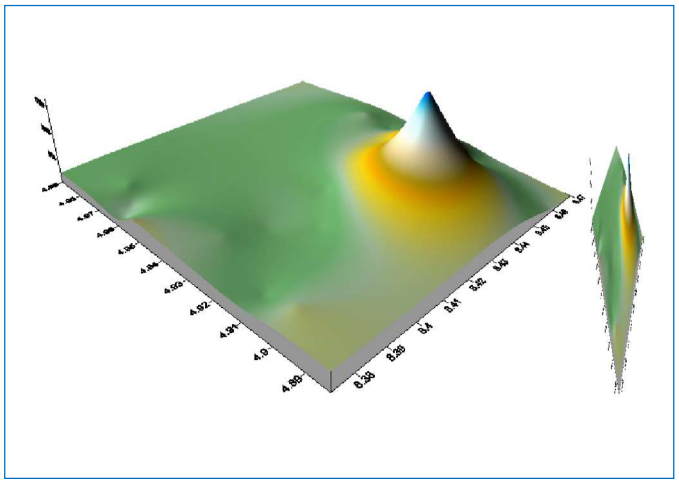

Fig. 17. Isograde plot of P distribution

Its similar good correlation with elements like Y, W, Ti, Ge, Cr and Cd is influenced by the similarities in their source and geochemical affinities, as attested to by the presence of moderately siderophile elements like W and Ge and slightly siderophile Cr. Arsenic is either non correlated or weakly correlated with other elements. A very good correlation is recorded between Au and Cs, K, Mg, and P. Other elements with a good correlation with Au are Zn, Ti, Sr, Na and Bi. The correlations of Au with other elements are very weak to non-correlation.

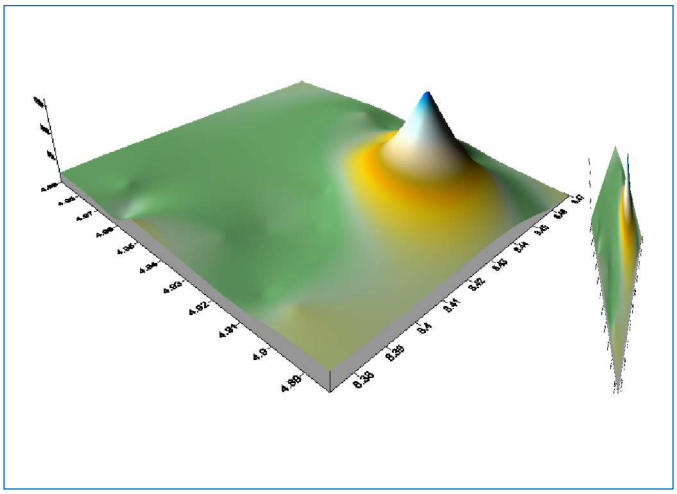

Fig. 18. Isograde plot of P distribution

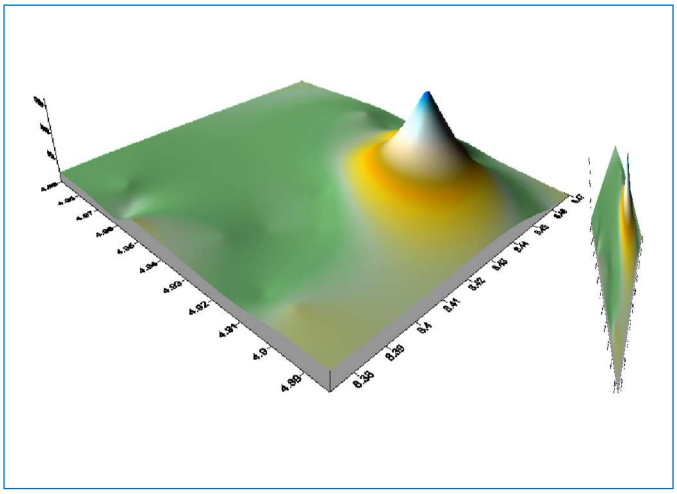

Fig. 19. Isograde plot of P distribution

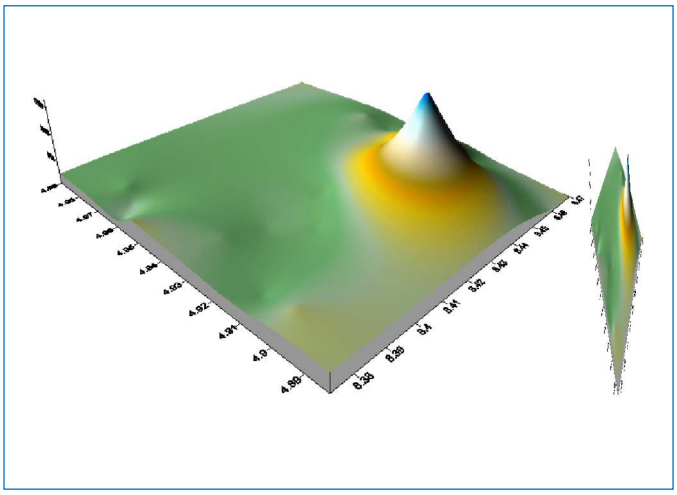

Fig. 12. Isograde plot of P distribution

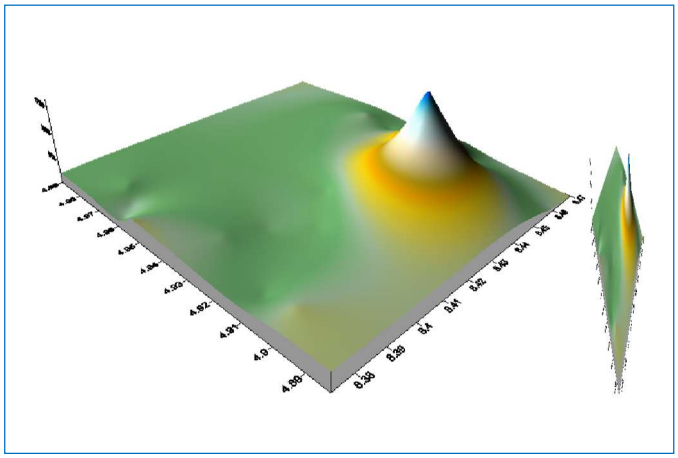

Fig. 12. Isograde plot of P distribution

The limited number of elements that are correlated with gold may be attributed to the inertness of this element, while its good correlation with Cs, K, Mg, P, Zn, Ti and Na is probably related to their presence in the same phase of mineralization as justified by their Factor Group. Other elements such as Bi (a chacophile element) and Sr (a lithophile element), have a good positive correlation with Au, which are probably because of their enrichments in the mineralizing fluid. Ce has an exceptionally good correlation with Co, Cu, Fe, Ga, Ge, Hf, In, La, Li, Mn, Ni, Pb, Th, Tl, V, W, Y and Zr. Other elements with good correlation with Ce are Cr, Te, U and Zn. Co. They also have a very good correlation with Cu, Ga, Li, Mn, Ni, Pb and Tl. Elements with a good correlation with Co include Y, V, Te, Na, Hf, Ge, Fe and Cr. Other elements with a good correlation with some of the correlated elements include Cr, Cs, Cu, Fe, Ga etc. Their exceptionally good correlation is aided by their association in most of the mineralization, while other elements have relatively low correlation with most of the correlated elements.

4. Conclusions

The conclusion drawn after integrating the field data, geochemical data, granulometric information and statistical results is that the area is mineralized. Based on the Factor group from statistical analyses and associated elements in the groups, it is concluded that the mineralizations in this area include low temperature sulphide minerals, gold and rare-earth metal mineralization. These rare-earth minerals are hosted in the pegmatite. From the isograde plots, it is concluded that the south and south-eastern part of the area is mineralized in gold and its associated minerals, while from the statistical analyses, it is concluded that pegmatites in the area host rare-earth mineralization that dominates the central and south-western parts of the area. The northern part of the study area, based on this work and isograde plots, is considered barren. Furthermore, from heavy mineral studies, heavy minerals such as sillimanite, rutile and zircon are good indicators of this mineralization. From the granulometric analysis, it was concluded that most of the stream sediments were deposited in low to high energy environment and are poorly sorted. The sediments were also sourced from different environments but deposited through settling or suspension.

Reference

Adam, E, Sean C.J., Amy, G., 2023. The applicability of G-BASE stream sediment geochemistry as a combined geological mapping, and prospective exploration tool for As-Co-Cu-Ni mineralisation across Cumbria, UK. Journal of Geochemical Exploration 253, 107297. https://doi.org/10.1016/j.gexplo.2023.107297.

Adekeye, J.I.D., 1999. Heavy minerals in stream sediments and their relationship to bedrock types and mineralization in Oro area, Southwestern Nigeria. Nigerian Journal of Pure and Applied Sciences 14, 906- 914.

Adekoya, J.A., Adeniji, M.O., Adesiyan, T.A., 2021. Reconnaissance Stream Sediment Geochemical Survey of Uokha Area, Southwestern Nigeria. Journal of Mining and Geology 57 (2), 339-349.

Awosusi, O.O., Adisa, A.L., Adekoya, J.A., 2019. Mineralization Potential Assessment of Stream Sediment Geochemical Data Using R-Mode Factor Analysis in Nigeria. International Journal of Scientific and Engineering Research 10 (12), 1055-1063.

Bamigboye, O.S., Adekeye, J.I.D., 2011. Sream sediment survey of Eruku and its environs, Central Nigeria: implication for exploration. International Journal of Research and Reviews in Applied Sciences 7 (2), 160-172.

Bamigboye, O.S., Bamidele, T.E., Omorinoye, O.A. Adeboye, J.O., 2023. Assessment of Mineralization Potential of Areas Represented on Ilorin Sheet 223, Southwestern Nigeria from Aeromagnetic and Aeroradiometric Analyses. Journal of Mining and Geology 59 (2), 117-129.

Berke, E.H., Spry, P.G., Heimann, A., Teale, G.S., Johnson, B., von der Handt, A., Alers, B., Shallow, J.M., 2023. The genesis of metamorphosed Paleoproterozoic massive sulphide occurrences in central Colorado: geological, mineralogical and sulphur isotope constraints. Geological Magazine 160, 1345-1375. https://doi.org/10.1017/S0016756823000407.

Boyle, R.W., 1974. Elemental associations in mineral deposits and indicator elements of interest in geochemical prospecting (Revised). Geological Survey of Canada Paper 74-45, 43p.

Chapman, J., Plouffe, A., Ferbey, T., 2015. Tourmaline: the universal indicator? 27th International Applied Geochemistry Symposium, Short Course, No. 2 p. 25-31.

Ekwueme, B.N., Shing, R., 1987. Occurrence, Geochemistry and Geochronology of mafic-Ultramafic rock in the Obudu Plateau S.E. Nigeria in Srivasta R.K. and Chadta, R. (eds) Magmatism relation to diverse tectonic settings. P. 293-306.

Folk, R.L., Ward, W.C., 1957. A Study in the Significance of Grain-Size Parameters. Journal of Sedimentary Petrology 27, 3-26.

Ghosh, B., Praveen, M.N., 2008. Indicator minerals as guides to base metal sulphide mineralisation in Betul Belt, central India. Journal of Earth System Science 117 (4), 521-536. https://doi.org/10.1007/s12040-008-0050-x.

Goldschmidt, V.M., 1954. Geochemistry. Oxford University Press, Oxford, England, 730 p.

Jones, H.A., Hockey, R.D., 1964. The geology of parts of Southwestern Nigeria. Geology Survey Nigerian Bulletin 31, 22-24.

Jun, H., Guanglu, M., Jing, Z., Jifei, C., Bin, W., Yanjun, L., Bo, Y., Xueqi, Z., Domenico, C., and the NGSSCA Project Team, 2024. National-scale Geochemical Survey: Distribution of chemical elements in stream sediment of South and Central Asia. Journal of Geochemical Exploration 262, 107452. https://doi.org/10.1016/j.gexplo.2024.107452.

Landergren, S., 1943. Geokemiska studier över Grängesbergsfältets järnmalmer. Plurabelle Books Ltd., Unit 8 Restwell House, Coldhams Rd, Cambridge, CB1 3EW, United Kingdom.

Levinson, A.A., 1981. Introduction to exploration geochemistry. Applied publishing Ltd, Wilmete, USA, 613 p.

McClenaghan, M.B., Parkhill, M.A., Pronk, A.G., 2015. Indicator mineral signatures of the Mount Pleasant Sn-W-Mo-Bi-In deposit, New Brunswick, Canada, 27th International Applied Geochemistry Symposium, Short Course No. 2, 63-79.

McClenaghan, M.B., Paulen, R.C., Smith, I.R., Rice, J.M., Plouffe, A., McMartin, I., Campbell, J.E., Lehtonen, M., Parsasadr, M., Beckett-Brown, C.E., 2023. Review of till geochemistry and indicator mineral methods for mineral exploration in glaciated terrain. Geochemistry: Exploration, Environment, Analysis 23, 1-43.

McCurry, P., Wright, J.B., 1977. Geochemistry of Calcalkaline volcanics in North-Western Nigeria and a possible Pan-African Suture Zone. Earth Planet Science Letters 37, 90-96. https://doi.org/10.1016/0012-821X(77)90149-2.

Obaje, O., Pirisola, A.O., 2023. Geochemical characterization of Egbetua stream sediments, southwestern Nigeria: implication for provenance and depositional conditions. British Journal of Earth Sciences Research, 11 (1), 17-30. https://doi.org/doi.org/10.37745/bjesr.2013.

Oraphan, Y., Shuyun X., Punya, C., Jianbiao, D., Weiji, W., 2023. Prediction of Au-Associated Minerals in Eastern Thailand Based on Stream Sediment Geochemical Data Analysis by S-A Multifractal Model. Minerals 13 (10), 1297. https://doi.org/10.3390/min13101297.

Ottesen, R.T., Theobald, P.K., 1994. Stream sediments in mineral exploration in Drainage Geochemistry edited by Hale, M. and Plant, J.A. Handbook of Exploration Geochemistry, Vol. 6 Elsevier Science,UK, pg 147-184.

Oyawoye, M.O., 1972. The Basement Complex of Nigeria. In: Dessauvagie, T.F.J., Whiteman, A.T. (eds.) African Geology, Ibadan, University Press, 66-102.

Rahaman, M.A., 1988. Recent Advances in the Study of the Basement Complex of Nigeria. In: Oluyide, P. O., Mbonu, W. C., Ogezi, A. E., Egbuniwe, I. G., Ajibade, A. C. and Umeji, A. C. (eds) Precambrian Geology of Nigeria. GNS 241-256.

Rahaman, M.A., Ocan, O., 1978. On relationships in the Precambrian migmatitic gneisses of Nigerian. Journal of Mining and Geology 15, 23-32.

Roache, T.J., Walshe, J.L., Huntington, J.F., Quigley, M.A., Yang, K., Bil, B.W., Blake, K.L., Hyvärinen, T., 2011. Epidote–clinozoisite as a hyperspectral tool in exploration for Archean gold, Australian Journal of Earth Sciences 58 (7), 813-822.

Russ, W., 1957. The Geology of parts of Niger, Zaria and Sokoto provinces. Bulletin (Geological Survey of Nigeria). No. 27.

Spry, P.G., McFadden, S., Teale, G.S., Alers, B., Shallow, J.M., Glenn, J.M., 2022. Nodular sillimanite rocks as field indicators to metamorphosed massive sulfide deposits. Ore Geology Reviews 141, 104632. https://doi.org/10.1016/j.oregeorev.2021.104632.

Stendal, H., Theobald, P.K., 1994. Heavy-mineral concentrates in geochemical exploration, In: Ale, H. and Plant, J.A. (eds) Drainage Geochemistry, Handbook of Exploration Geochemistry 6, 185-225.

Truswell, J.F., Cope, R.N., 1963. The Geology of parts of Niger and Zaria Provinces. Northern Nigeria. Bulletin (Geological Survey of Nigeria). No. 29.

Zhihua, W., Jun, H., Xin, L., Huishan, Z., Yasir, S.K., Naghma, H., Mehboob, U.R., Muhammad, J.Z., Asad, A.N., 2024. Concentration and distribution patterns of rare earth elements (REEs) in stream sediments of Pakistan, Journal of Geochemical Exploration 258, 107386, https://doi.org/10.1016/j.gexplo.2024.107386.